Int. J. Heat Mass Transfer. Vol. 36, No. 9, pp. 2375–2384, 1993
Printed in Great Britain

0017-9310/93 $6.00+0.00

Numerical analysis of mixed convection at the entrance region of a rectangular duct heated from below

U. NARUSAWA
Department of Mechanical Engineering, Northeastern University, Boston, Massachusetts 02115, U.S.A.

(*Received* 30 *April* 1992 *and in final form* 4 *September* 1992)

Abstract—An entrance region of a rectangular duct is examined numerically for a thermally-developing flow between a cooled top and a heated bottom boundary. Based on the results, which agree well with previous experimental results, equations for the entrance lengths, L_1 for the onset and L_2 for the full development of mixed convection are proposed. L_1 approximately corresponds to the location where the Nusselt number takes a minimum before is increases as the buoyancy-induced flow becomes dominant. Results on the effects of the sidewall thermal condition as well as the inlet gas temperature are also discussed in relation to thermal transport.

INTRODUCTION

LAMINAR flow and heat transport in the entrance region of a duct has been investigated extensively in the past in relation to various practical applications, particularly for the design of heat exchangers. More recently, chemical vapor deposition of a thin film has been the subject of importance in semiconductor manufacturing processes. In some of these processes, chemical reactions occurring in a reactor chamber consisting of a rectangular duct are strongly dictated by thermofluid conditions, which affect uniformity and the growth rate of the deposited film, thereby making the understanding of the entrance region of a duct all the more important.

Beavers *et al.* [1] reported carefully-obtained experimental results of pressure drop for hydrodynamically developing (cold) flow in rectangular ducts for various values of the aspect ratio. For laminar forced convection in channels, Shah and London [2] provide an extensive compilation of various works, including experimental and numerical results as well as available exact solutions. Buoyancy effects in laminar flow in a horizontal channel are important because of the possible substantial enhancement in heat transfer due to a buoyancy-driven secondary flow. On the other hand, in CVD reactors the presence of a secondary flow may have adverse effects on the uniform deposition of a film. Experimental studies are reported on the onset of mixed convection in horizontal ducts by many investigators, including Akiyama *et al.* [3], Hwang and Cheng [4], Kamotani and Ostrach [5] and Kamotani *et al.* [6]. (See Incropera and Schutt [7] and Chiu and Rosenberger [8] for additional papers, relevant to this subject.) These studies confirm the existence of a regular, time-dependent, buoyancy-driven cross flow in low Rayleigh number flows. Theoretical (numerical) results of the thermal entrance region of a channel are also available. Ou *et al.* [9] analyzed the problem for a large Prandtl number fluid, which allows one to neglect convective terms in governing equations. With the convective terms retained, mixed convection in the entrance region of a horizontal channel was analyzed by Abou-Ellail and Morcos [10] for a uniform surface heat flux. More recently, Incropera and Schutt [7] studied the entrance region, examining the effects of various factors (such as the magnitudes of the Prandtl number and the Rayleigh number, thermal or combined (simultaneous) entrance, and the surface thermal condition) on heat transfer. Experimental studies by laser Doppler anemometry using nitrogen gas are reported in two successive papers (Chiu and Rosenberger [8] and Chiu *et al.* [11]), in which both thermally-developing and fully-developed flows are investigated for mixed convection between horizontal plates heated from below. Based on their experiments they proposed explicit expressions for the entrance length for the onset of buoyancy-driven convective instability as well as for the full development of the mixed flow. Furthermore, time-dependent convection rolls in the main flow direction are observed for a flow with a high-Rayleigh number and a low-Reynolds number. In relation to silicon CVD in horizontal reactors, Moffat and Jensen [12, 13] performed numerical analyses for a thermally-developing entrance flow in a rectangular duct. (See also Jensen *et al.* [14, 15].) Their study takes into account buoyancy effects without the Boussinesq approximation, and density variations as well as property changes with temperature. Their numerical results for nitrogen gas predict the entrance length for the full-development of the mixed flow that agrees well with the corresponding experimental results of Chiu and Rosenberger [8].

NOMENCLATURE

AR	aspect ratio, $2\cdot Wd/H$
C_p	specific heat at constant pressure
D_h	hydraulic diameter
D_T	thermal diffusivity
g	gravitational acceleration
H	height of a duct
k	thermal conductivity
L_1	entrance length for the onset of mixed convection
L_2	entrance length for the full development of mixed convection
Nu	average Nusselt number at the bottom, $D_h\cdot\overline{(\partial T/\partial y)_{bot}}/(T_{bot}-T_m)$ with $\overline{(\partial T/\partial y)_{bot}}$ being the temperature gradient at the bottom averaged over the half-width
Nu_{min}	minimum Nusselt number
Nu_{ss}	Nu of fully-developed mixed convection
p	pressure
P_0	absolute pressure of gas at the inlet
Pr	Prandtl number, based on $T = T_i$
R	gas constant
Ra	Rayleigh number, $g(\Delta\rho/\rho)H^3/\nu\alpha$, with ν and α evaluated at $(T_{bot}+T_i)/2$
Ra_c	critical Rayleigh number for the Rayleigh–Bénard convection (= 1708)
Re	Reynolds number, $w_0\cdot H/\nu$ with ν evaluated at $T=(T_{bot}+T_i)/2$
Re_D	Reynolds number, $\bar{w}\cdot D_h/\nu$ with ν evaluated at $T = T_i$
T	temperature
T_i	gas temperature at the inlet, $z = 0$
T_m	mixing-cup temperature
T_s	temperature of the sidewall
T_{bot}	temperature of the bottom boundary
T_{top}	temperatures of the top boundary
ΔT	$(T_i-T_{top})/(T_{bot}-T_{top})$
u	velocity in x (lateral)- direction
v	velocity in y (vertical)- direction
w	velocity in z (main flow)- direction
w_0	maximum velocity at the inlet, divided by 1.5
$\bar{w}$	average velocity at the inlet
Wd	half-width of a duct
ΔW	fraction of the deviation of $w(x/Wd = \sim 0.5, y/H = 0.2, z)$ from $w(x/Wd = 0.5, y/H = 0.2, z = 0)$
$\Delta WMOD$	fraction of the deviation of the modulation amplitude of x at $(x/Wd = \sim 0.5, y/H = 0.5, z)$ from the corresponding value of the fully-developed flow
x	transverse coordinate
y	vertical coordinate
z	longitudinal coordinate
z^+	inverse Graetz number, $z/(D_h\cdot Re_D\cdot Pr)$.

Greek symbols

θ	non-dimensional temperature, $(T-T_{top})/(T_{bot}-T_{top})$
θ_m	non-dimensional mixing-cup temperature
μ	absolute viscosity
ν	kinematic viscosity
ρ	density
$\Delta\rho$	density difference corresponding to the temperature difference between the top and the bottom boundaries.

These studies indicate that a numerical approach could provide significant insight into the hydrodynamic and thermal structure at the entrance region of rectangular ducts. The present study attempts to extend numerical analyses further for a more detailed understanding of flow behavior particularly in relation to thermal transport, with the previously-reported experimental results utilized to determine the accuracy and limitations of our study.

FORMULATION AND METHOD OF SOLUTION

We consider a horizontal rectangular duct of a cross-sectional area, $2\cdot Wd\times H$ (the aspect ratio $AR = 2\cdot Wd/H$), with the coordinate system (x, y, z) set up in the directions of the width, the height and the main flow respectively with its origin at the bottom corner of the inlet section. At $z = 0$ a hydrodynamically-developed, isothermal gas flow enters the duct in which the top and the bottom boundaries are respectively cooled and heated isothermally, while the sidewalls are either insulated or maintained at a specified temperature. (Some of the thermal boundary conditions are altered during our study to examine effects of these conditions on entrance lengths.) The formulation presented below is written under the following assumptions:

(1) The flow is steady.
(2) The ideal gas equation of state with constant pressure is valid to evaluate density variations in the flow.
(3) The viscous dissipation and the compressibility effect (i.e. the term $\propto (Dp/Dt)$ for flow energy) are negligible in the energy equation.
(4) The diffusion in the z (main flow) direction is neglected in momentum and energy conservation equations [16]. For the present flow in an inlet section of a duct, cross-stream (xy-plane) flow is generated by buoyancy. When

the velocity components in the cross-stream direction are small compared to the main flow velocity, it may be shown from a dimensional argument that convection dominated over diffusion in the z direction.

Assumption (2) is valid in relation to the pressure change with flow in the duct since the pressure drop near the entrance of a duct may be much smaller than the magnitude of pressure at the inlet. This also implies that density changes due solely to a change in temperature. Then the governing equations are,

Continuity:

$$\frac{\partial(\rho u)}{\partial x}+\frac{\partial(\rho v)}{\partial y}+\frac{\partial(\rho w)}{\partial z}=0. \tag{1}$$

Conservation of momentum:

$$\rho\left(u\frac{\partial u}{\partial x}+v\frac{\partial u}{\partial y}+w\frac{\partial u}{\partial z}\right)=-\frac{\partial p}{\partial x}+\frac{\partial}{\partial x}\left(\mu\frac{\partial u}{\partial x}\right)+\frac{\partial}{\partial y}\left(\mu\frac{\partial u}{\partial y}\right)+\frac{\partial}{\partial x}\left(\mu\frac{\partial u}{\partial x}-\frac{2}{3}\mu\left(\frac{\partial u}{\partial x}+\frac{\partial v}{\partial y}+\frac{\partial w}{\partial z}\right)\right)+\frac{\partial}{\partial y}\left(\mu\frac{\partial v}{\partial x}\right)+\frac{\partial}{\partial z}\left(\mu\frac{\partial w}{\partial x}\right), \tag{2}$$

$$\rho\left(u\frac{\partial v}{\partial x}+v\frac{\partial v}{\partial y}+w\frac{\partial v}{\partial z}\right)=-\frac{\partial p}{\partial y}+\frac{\partial}{\partial x}\left(\mu\frac{\partial v}{\partial x}\right)+\frac{\partial}{\partial y}\left(\mu\frac{\partial v}{\partial y}\right)+\frac{\partial}{\partial x}\left(\mu\frac{\partial u}{\partial y}\right)+\frac{\partial}{\partial y}\left(\mu\frac{\partial v}{\partial y}-\frac{2}{3}\mu\left(\frac{\partial u}{\partial x}+\frac{\partial v}{\partial y}+\frac{\partial w}{\partial z}\right)\right)+\frac{\partial}{\partial z}\left(\mu\frac{\partial w}{\partial y}\right)-\rho g, \tag{3}$$

$$\rho\left(u\frac{\partial w}{\partial x}+v\frac{\partial w}{\partial y}+w\frac{\partial w}{\partial z}\right)=-\frac{\partial p}{\partial z}+\frac{\partial}{\partial x}\left(\mu\frac{\partial w}{\partial x}\right)+\frac{\partial}{\partial y}\left(\mu\frac{\partial w}{\partial y}\right). \tag{4}$$

Conservation of energy:

$$\rho C_p\left(u\frac{\partial T}{\partial x}+v\frac{\partial T}{\partial y}+w\frac{\partial T}{\partial z}\right)=\frac{\partial}{\partial x}\left(k\frac{\partial T}{\partial x}\right)+\frac{\partial}{\partial y}\left(k\frac{\partial T}{\partial y}\right). \tag{5}$$

Equation of state:

$$\rho = P_0/RT. \tag{6}$$

In the set of momentum equations above, the downstream effects are transmitted upstream through the pressure variation, ∇p. The final, fully-parabolized, governing equations may be obtained by setting $p=\bar{p}(z)+p'(x,\ y,\ z)$ under the assumption of $\mathrm{d}\bar{p}/\mathrm{d}z \gg \partial p'/\partial x,\ \partial p'/\partial y,\ \partial p'/\partial z$. The resulting changes in conservation of momentum are,

$$\partial p/\partial x \to \partial p'/\partial x,\quad \partial p/\partial y \to \partial p'/\partial y,\quad \partial p/\partial z \to \mathrm{d}\bar{p}/\mathrm{d}z. \tag{7}$$

It should also be mentioned here that in evaluating the buoyancy term, the Boussinesq approximation is not applied because of possible large density changes present in the duct. Both viscosity and thermal conductivity are given as functions of temperature, while specific heat at constant pressure is assumed constant.

Because of symmetry with respect to $x = Wd$, computation is performed over half the cross-section of a duct between $x = 0$ and Wd. Hence the hydrodynamic and thermal boundary conditions become,

$$u = v = w = 0 \quad \text{at the top, bottom and side bounding walls} \tag{8}$$

$$u=\frac{\partial v}{\partial x}=\frac{\partial w}{\partial x}=0 \quad \text{at} \quad x = Wd \tag{9}$$

$$\frac{\partial T}{\partial x}(x=0,y,z)=0,$$

or

$$T(x=0,y,z)=T_s(\text{specified}) \tag{10}$$

$$\frac{\partial T}{\partial x}(x=Wd,y,z)=0 \tag{11}$$

$$T(x,y=0(H),z)=T_{\text{bot(top)}}(\text{specified}). \tag{12}$$

Since the pressure gradient in the z direction is decoupled from that in the x-, y-directions, computation for a given set of entrance conditions for $\mathbf{V}$-, and T-fields, marches downstream at an interval of Δz, and at each z location, T and w, and u and v are evaluated one by one before proceeding to the next z location. The calculation domain is divided into a number of finite control volumes, each surrounding a grid point. The conservation equations are integrated over the control volume. The set of discretized equations, thus generated, is based on a staggered grid system, in which pressure, temperature and w (streamwise velocity) are calculated at main grid points, while u and v cross-stream velocities in the x and y directions, respectively) are evaluated at secondary grid points. The momentum and energy equations are linearized by using upstream values to calculate coefficients of the discretized equations. The convection-diffusion fluxes that appear in the discretized equations are evaluated by employing the 'hybrid' scheme. (See Patankar [17].) The grid system is based on variable spacings with finer meshes near the boundaries. A solution to a set of linear discretized equations is obtained by using the line-by-line TDMA(Tri-Diagonal Matrix Algorithm).

For the solution to momentum and energy equations at a given z location, the energy equation is solved first to find the temperature (and density) field. A value of $d\bar{p}/dz$ is assumed to obtain the corresponding w field from the momentum equation in the z direction. Based on this w field, the overall continuity requirement of specified mass flow rate is checked. Then, the pressure gradient is corrected from the computed excess mass to iterate the procedure until the overall continuity is satisfied. In order to obtain the cross-stream velocity field from momentum equations in the x and y directions, we used an algorithm, called SIMPLER [17]. In this algorithm a pressure field is obtained first as a solution to the pressure equation constructed from a guessed cross-stream velocity field. Based on this pressure field, the momentum equations are solved for the u and v fields. The results are then used to check the local continuity requirements. The cross-stream velocity field is then corrected from a solution to the 'pressure-correction' equation, which is derived from the local excess mass, and the procedure is repeated until local continuity is satisfied at all grid points.

RESULTS AND DISCUSSION

Following the dimensions used by Chiu and Rosenberger [8] for their experimental studies, the duct of our analyses has physical dimensions of H (height) $\times$ Wd (half-width) $= 15.8 \times 79$ mm with the aspect ratio, AR $(=2Wd/H)$, of 10. Nitrogen gas (with the Prandtl number, $Pr = \sim 0.71$) is used for the present analyses. Density, viscosity and thermal conductivity of nitrogen gas vary a maximum of $\sim 15\%$ over the temperature range of 300–350 K, corresponding to the Rayleigh number covered in the analyses. Based on the accuracy test as well as comparisons with experimental results discussed below, a mesh of 27 (in the x direction) $\times$ 10 (in the y direction) and the z-direction increment, Δz, of 0.5 mm are employed with the spacing between grid points varying smoothly within the range of 1.0–3.0 mm. A finer mesh did not alter our results in terms of the entrance lengths to be discussed below. Although the computer time requirements depend on how far downstream the computation is performed, a typical run required 3000–4000 CPU seconds using a SUN SPARC workstation. A discussion of results, which follows the accuracy tests of our program, consists of comparisons between the present results with experimental data, and examinations of various factors affecting flow near the entrance region as well as of the flow structure in relation to thermal transport.

To test the validity of our program, pressure variations along a rectangular duct are computed first for a hydrodynamically developing isothermal flow. Our results, obtained for ducts of $AR = 1$, 2, 5 and 10, showed very good agreement with the experimental results of ref. [1]. Then fully-developed velocity profiles for an isothermal flow in rectangular ducts are compared with the exact solution [2], followed by a comparison of variations of the local Nusselt number (averaged over the cross-section) with previous numerical results of ducts with $AR = 1$, 2 and 4 for thermally developing, and hydrodynamically developed forced convection flow with all four walls kept at a constant temperature [2]. Excellent agreements are confirmed for both the velocity profiles of the cold flow and the variations of the Nusselt number. For a flow between parallel plates heated at the bottom and cooled at the top, forced convection prevails for $Ra < Ra_c$ $(=1708$, the critical Rayleigh number for the onset of steady convection in the Rayleigh–Bénard geometry). When instability sets in, longitudinal convective rolls appear with their w velocity profile having a wavelength of $2H$. These rolls are steady for $Ra_c < Ra < Ra_{cc}$, where Ra_{cc} is the second critical Rayleigh number above which the flow becomes time-dependent. Chiu and Rosenberger [8] found in their experimental investigation that the magnitude of Ra_{cc}, which is a function of the Reynolds number, is much higher than the corresponding critical Rayleigh number for the Rayleigh–Bénard convection [18], indicating that the presence of forced convection suppresses the onset of instability. The reference conditions are:

a thermally developing flow of nitrogen gas,
Wd (duct half-width) $= 79$ mm, H (duct height) $= 15.8$ mm,
AR (aspect ratio) $= 10$,
adiabatic sidewalls,
T_i (inlet gas) $= T_{top}$ (the top boundary) $= 300$ K,
T_{bot} (the bottom boundary) $> T_{top}$.

Unless stated otherwise, the results presented below are obtained under the reference conditions. The Rayleigh number and the Reynolds number are defined as,

$$Ra = \frac{gH^3 \Delta\rho/\rho_{in}}{\nu D_T}, \quad Re = \frac{w_0 H}{\nu}$$

where $w_0 = w_{max}/1.5$ with ν and D_T being evaluated at $T = (T_i + T_{bot})/2$.

Ranges of Ra and Re in the present study are, $\sim 2400 < Ra < \sim 8500$ (with the corresponding temperature difference, $T_{bot} - T_{top}$, of 10–40 K) and $\sim 20 < Re < \sim 200$. The lower limit for Re arises from the consideration that for $Re \sim 10$ both longitudinal diffusion and a local backflow due to gas expansion may be important [16], the effects of which are not accounted for in the present fully-parabolized formulation. It should also be mentioned here that a second Reynolds number, Re_D, is introduced later when an inverse Graetz number is defined.

Chiu and Rosenberger [8] measured two kinds of entrance lengths, L_1 and L_2 for a thermally developing nitrogen gas flow in a rectangular duct of the same dimensions as the present analyses with adiabatic sidewalls. L_1 (the entrance length for the onset of buoyancy-driven convection) is defined as the distance

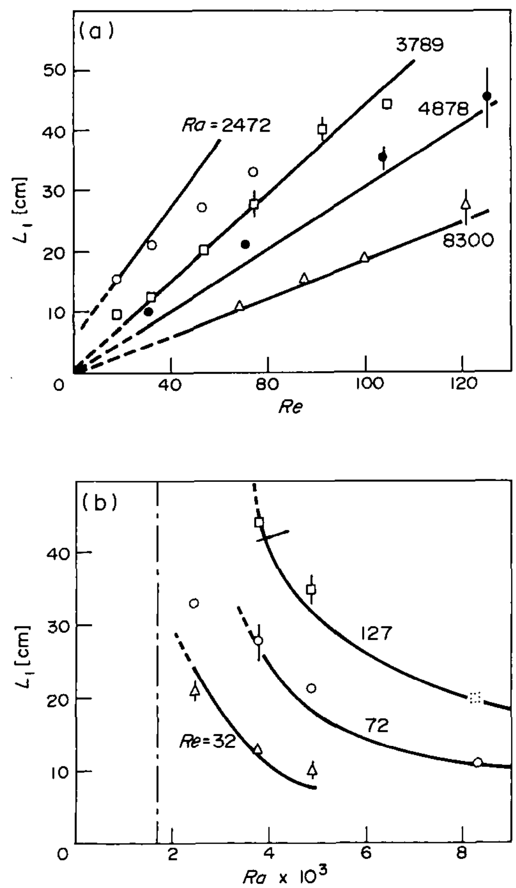

FIG. 1. Comparison between the computed entrance length, L_1, and experimental results [8]. (a) L_1 vs Re for specified values of Ra. ○ : Ra = 2472, □ : Ra = 3789, □ : Ra = 3789, ● : Ra = 4878, △ : Ra = 8300. (b) L_1 vs Ra for specified values of Re. □ : Re = 127.3–129.49. (The data point given as a dotted square is interpolated from the experimental data for Ra = 8300.) ○ : Re = 68.3–74.5, △ : Re = 31.6–32.5. The vertical broken line at Ra = 1708 indicates the critical Rayleigh number for the onset of convection for Rayleigh–Bénard convection.

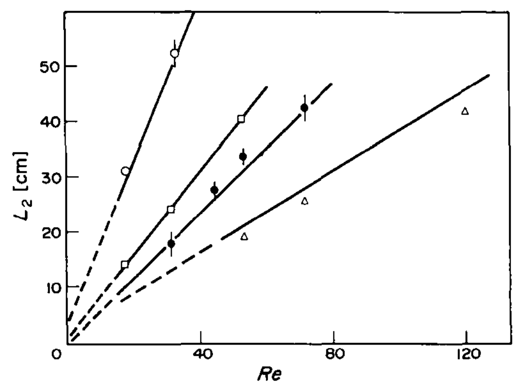

FIG. 2. Comparison between the computed entrance length, L_2, and experimental results as L_2 vs Re for specified values of Ra. (See Fig. 1(a) for the symbols used for experimental data points [8].)

from the entrance to a point where the change of the w-velocity profile in the central region at $y/H = 0.2$ exceeds 3% of $w(x/Wd = 0.5,\ y/H = 0.2,\ z = 0)$; while L_2 (the entrance length for full development of the mixed flow) is defined as the distance from the entrance to a point where the modulation amplitude of the w-velocity profile at $y/H = 0.5$ in the central region of the channel, reaches 95% of the modulation amplitude of the w-velocity profile in the fully-developed region. Numerical results of L_1 and L_2 are shown in Figs. 1 and 2 along with the corresponding experimental results in ref. [8], with the solid lines indicating ranges of the numerical analyses. Both L_1 and L_2 may be linearly dependent on the Reynolds number for a given value of the Rayleigh number, with the differences between computed values of L_1 and L_2 and the lines shown in Figs. 1(a) and 2 being less than ± 1 cm. In Fig. 1 it may be seen that the numerical prediction for L_1 shows good agreement with the experimental results except for the case of $Ra = 2472$. It should also be mentioned here that our results for L_1 are well within the maximum/minimum ranges of the empirical relation of L_1/H as a function of Re, Ra and Ra_c, obtained through a least square fit to the data points in ref. [8]. Furthermore, the results for L_2 depicted in Fig. 2 show very good agreement with experiments. The computed values of L_2 for $Ra = 8300$ lie slightly above the corresponding experimental data points, which could be attributed to our fully-parabolized governing equations since cross-sectional pressure variations increase with the Rayleigh number. Figure 3(a) is a sketch of a typical variation of the midplane longitudinal velocity, $w(0 \leqslant x \leqslant Wd,\ y = H/2,\ z)$ over a half-width (with an adiabatic wall located at $x/H = 0$) at selected locations in the mainflow (z) direction. The instability initially occurs near the adiabatic sidewall due to horizontal temperature gradients as shown experimentally. Velocity and temperature profiles are modulated in the presence of buoyancy-induced crossflow. When a fully-developed state is reached, there are five roll cells over the half-width with wavelengths of H (=duct height) for modulated w profiles and $2H$ for modulated temperature profiles. Table 1 lists some typical values of the modulation amplitude of w at the midplane of $y = H/2$, $\Delta WMOD$, along with the corresponding experimental results by Chiu *et al.* [11]. Our numerical values of $\Delta WMOD$ are obtained from interpolation of the w-velocities at grid points near the center of the duct. Although the modulation amplitude increases sharply with an increase in the Rayleigh number, making the interpolation (from our coarse grid spacing relative to the wavelength) less accurate, our numerical results are generally in good agreement with the experiments. Based on these results, it is concluded that our numerical approach provides a good picture of thermofluid behavior in the region where steady convective rolls are generated by buoyancy.

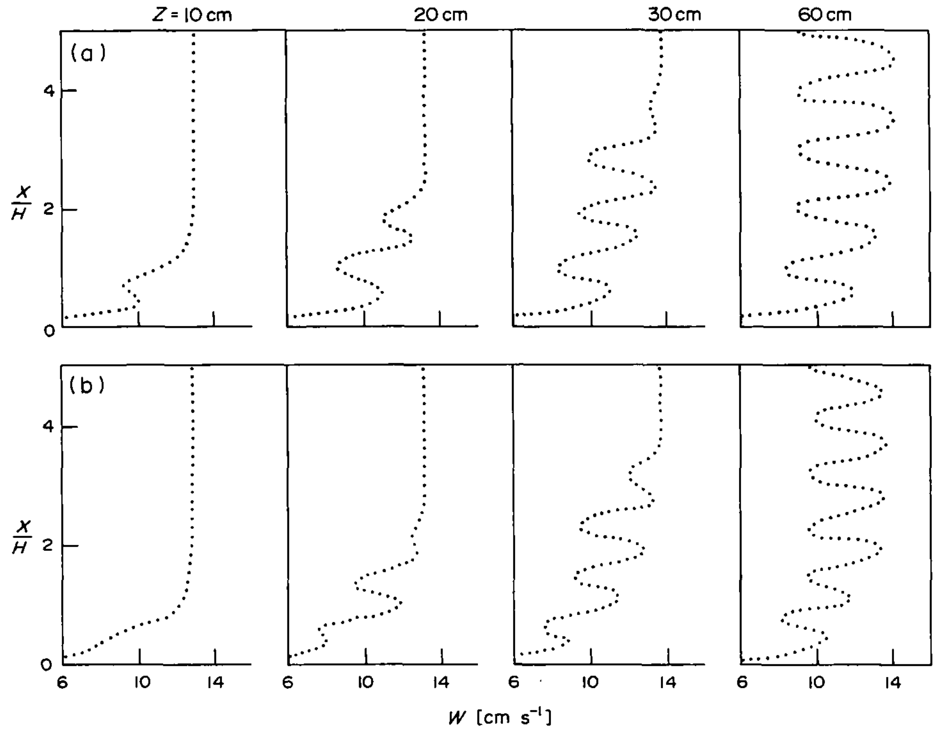

FIG. 3. Propagation of disturbance for $Ra = 6446$, $Re = 80$. (a) adiabatic sidewalls, (b) isothermal sidewalls ($T_s = T_i = T_{top}$).

In order to examine effects of thermal conditions at the sidewalls where buoyancy-induced motion originates, several computational results are obtained, in which a condition of constant sidewall temperature is imposed instead of the adiabatic condition. The entrance lengths for the cases of $T_{top} = T_s > T_{bot}$ are found to be slightly shorter with the maximum deviation from the cases of the adiabatic sidewalls of $\sim 10\%$ under the conditions of a low Rayleigh number ($\lesssim 4000$) and a high Reynolds number ($\lesssim 100$). Figure 3(b) shows typical variations of the midplane longitudinal velocity over a half-width for the case of isothermal sidewalls. It should be noted that there are six roll cells over the half-width, compared to five cells for the case of the adiabatic sidewalls shown in Fig. 3(a). Unlike the Rayleigh–Bénard geometry, a cold vertical sidewall bounded by a cold top and a hot bottom plate is expected to readily induce buoyancy-driven flow. This may be a cause of some adjustment in the cell arrangement different from the prediction made for the Rayleigh–Bénard convection. When the temperature of the entering flow is different from the temperature of the top bounding plate, one may expect changes in the magnitudes of L_1 and L_2. Defining $\Delta T = (T_i - T_{top})/(T_{bot} - T_{top})$, computations are performed for $\Delta T = \pm 1/2$. When $\Delta T = 1/2$ (i.e. the entering flow has a higher temperature than the temperature of the top boundary), the 'effective' Rayleigh number is reduced near the entrance due to a smaller temperature difference between the entering flow and the bottom plate; hence we may expect a greater entrance length, L_1. On the other hand, when $\Delta T = -1/2$ a buoyancy-induced secondary flow should be generated more readily due to a greater temperature difference between the inlet flow and the bottom boundary. The effects of the entering flow temperature on L_1 and L_2 are shown in Fig. 4, in which conditions, other than the value of ΔT, are the same as the reference conditions. Again the Reynolds number dependencies of L_1 and L_2 are well represented by linear relations for a fixed value of the Rayleigh number over the range of our investigation. Significant changes are observed for L_1 for both $Ra = 3789$ and 4878, with

Table 1. Comparison of modulation amplitude of w, $\Delta WMOD$, in [cm s^{-1}] for fully-developed flow at the midplane, $y = H/2$

Ra	*Re*	This work	Experiment†	
2472	18.1	0.24	0.24‡	0.29§
	32.5	0.42	0.41	0.45
3789	31.8	0.65	0.71	
	53.8	1.04	1.06	1.36
4878	52.8	1.64	1.60	1.68
	71.7	2.15	1.88	
6446	53.4	1.92		1.88
	71.3	2.44		2.56
8300	53.4	2.24	2.54	2.37
	71.7	3.02	3.20	2.96

† from Chiu *et al.* [11].
‡ LDV beam spacing of 50 mm.
§ LDV beam spacing of 22 mm.

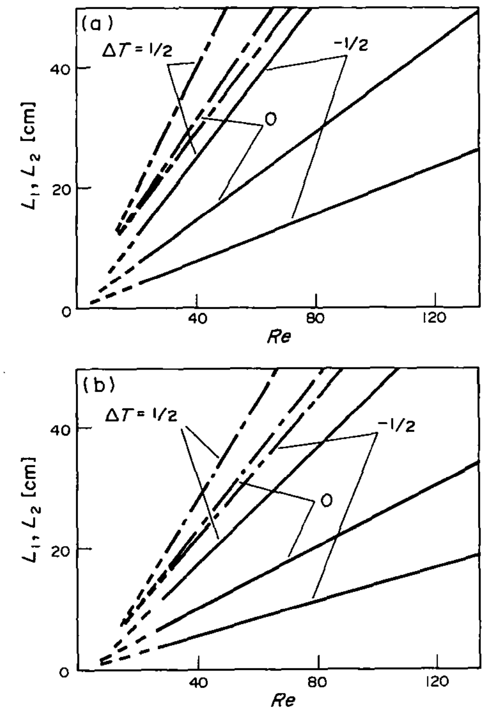

FIG. 4. Effects of inlet gas temperature on L_1 and L_2 for $Ra = 3789$ and $Ra = 4878$ with solid- and broken-lines representing L_1 and L_2 respectively.

the magnitude of L_1 when $\Delta T = -1/2$, decreasing to 50–60% of the corresponding values of L_1 under the reference conditions (i.e. $\Delta T = 0$), and increasing to 150–180% of $L_1(\Delta T = 0)$ when $\Delta T = 1/2$, over the range of the Reynolds number shown in the figure. The effect of ΔT values on L_2 is not as significant as that on L_1, particularly for the case of $\Delta T = -1/2$, in which the reduction in L_2 is less than $\sim 10\%$. In Fig. 5 are sketched typical variations of ΔW and $\Delta WMOD$ when ΔT takes three different values of $-1/2$, 0, 1/2 for the case of $Ra = 3789$ and $Re = 51$. ΔW is a fraction of the deviation of $w(x/Wd = \sim 0.5$, $y/H = 0.2$, $z = z)$ from $w(x/Wd = 0.5$, $y/H = 0.2$, $z = 0)$ at the inlet. (The z location in which ΔW is 3%

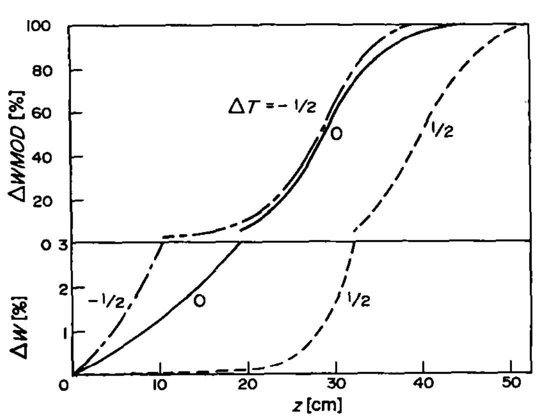

FIG. 5. Developments of $\Delta WMOD$ and ΔW for $Ra = 3789$, $Re = 51$.

is defined as L_1.) On the other hand, $\Delta WMOD$ is a fraction of the deviation of the modulation amplitude of w velocity profile at $x/Wd = \sim 0.5$, $y/H = 0.5$, $z = z$, from the corresponding modulation amplitude of the fully-developed region downstream. (The z location where $\Delta WMOD$ is 95% is defined as L_2.) When the inlet gas temperature is lower than that of the top bounding wall (i.e. $\Delta T = -1/2$), the slope of the rise in ΔW becomes greater, compared to the reference case of $\Delta T = 0$. On the other hand, when the inlet gas has a higher temperature than the top bounding wall (i.e. $\Delta T = 1/2$), an evolution of ΔW is delayed considerably due to suppression of the onset of convective instability with a low 'effective' Rayleigh number. A sharp increase in buoyancy-induced motion in terms of the magnitude of $\Delta WMOD$ is similar in their rising profiles once the values of $\Delta WMOD$ reaches $\sim 5\%$. It should also be mentioned here that an increase in L_2 when $\Delta T = 1/2$ is strongly related to a delay in the development of L_1.

The onset of buoyancy-induced secondary flow will now be examined in relation to thermal transport. It has been shown that our results for L_1 and L_2 are linearly dependent on the Reynolds number for a fixed value of the Rayleigh number. Incropera and Schutt [7] showed through their numerical analyses that the inverse Graetz number, z^+, is an appropriate length scale for the study of mixed convection at the entrance of a duct. The inverse Graetz number is defined as the z direction coordinate divided by the product of the hydraulic diameter, D_h, the Prandtl number, Pr, and a Reynolds number based on D_h and the average flow velocity at the inlet, Re_D (i.e. $z^+ = z/D_h \cdot Pr \cdot Re_D$). Although our analysis entails variable properties, it is confirmed that values of $z^+_{L_1}$ and $z^+_{L_2}$ (the corresponding inverse Graetz numbers for L_1 and L_2 respectively with property values evaluated at the inlet gas temperature) are indistinguishable from each other when the Reynolds number is varied for given value of the Rayleigh number with the differences among them being less than 3%. Computed values of $z^+_{L_1}$ and $z^+_{L_2}$ are shown as two broken lines in Fig. 7(b) as functions of Ra. These two curves may be represented by the following two equations with the deviations from the curves of less than 4%;

$$z^+_{L_1} = 0.114((Ra - Ra_c)/Ra_c)^{-0.764}, \tag{13}$$

$$z^+_{L_2} = 0.245((Ra - Ra_c)/Ra_c)^{-0.670}. \tag{14}$$

To examine thermal transport, the Nusselt number, Nu, at the bottom, averaged over the cross-sectional length may be defined as

$$Nu = \frac{D_h \cdot \overline{(\partial T/\partial y)}_{bot}}{(T_{bot} - T_m)}$$

where $\overline{(\partial T/\partial y)}_{bot}$ is the temperature gradient at the bottom, averaged over the half-width, Wd, at a fixed z location, and T_m is the mixed mean fluid temperature.

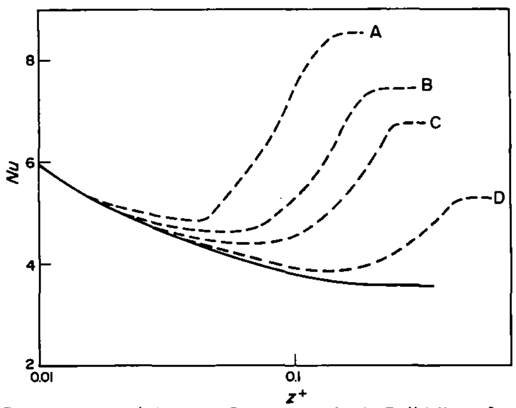

FIG. 6. Nu vs z^+(inverse Graetz number). Solid line: forced convection, Broken lines A, B, C, D for Ra = 8144, 4926, 3777, 2461 respectively.

Figure 6 shows some typical variations of Nu with the inverse Graetz number. Again the effects of temperature-dependent properties cause deviations in Nu of less than 5% about the curves shown in Fig. 6, indicating that Nu is essentially independent of the Reynolds number. The bottom Nusselt number starts to deviate from the corresponding forced convection value (solid line), attaining a minimum, then increases downstream, eventually reaching a fully-developed value. Figure 7(a) depicts the bottom Nusselt number at the minimum point (Nu_{min}, the broken line) and the Nusselt number for a fully-developed flow (Nu_{ss}, the solid line) over our range of analyses of Ra = 2400–8500. The buoyancy-induced secondary flow enhances heat transfer substantially as we compare Nu_{ss} with the Nusselt number for (subcritical) forced convection (~ 3.57). It should also be noted that as Ra increases, the curves of both Nu_{ss} and Nu_{min} become more flattened. Figure 7(a) also shows Nu_{ss} (dotted line) for fully-developed mixed convection between the heated bottom and the cooled top (i.e. the case of $AR \to \infty$) [19]. The Nusselt number of the duct with $AR = 10$ is seen to be lower than the corresponding value of mixed convection between two flat plates by 8–10% due to the effect of sidewalls on thermofluid structure.

To understand the locations of L_1 and L_2 in relation to heat transport, the inverse Graetz numbers are obtained for the location of Nu_{min} as well as the location where 95% of the Nusselt number of a fully-developed flow is reached—each defined as $z^+(Nu_{min})$ and $z^+(95\% Nu_{ss})$. They are plotted in Fig. 7(b) along with $z^+_{L_1}$ and $z^+_{L_2}$. While the difference between $z^+_{L_1}$ and $z^+(Nu_{min})$ becomes smaller as the Rayleigh number increases, $z^+_{L_2}$ is roughly the same in magnitude as $z^+(95\% Nu_{ss})$ over the range of the Rayleigh number in our study. Figure 8 presents developments of both the Nusselt number and the non-dimensional mixed mean fluid temperature, $\theta_m (= (T_m - T_{top})/(T_{bot} - T_{top}))$ along with the locations of $z^+_{L_1}$, $z^+_{L_2}$, $z+(Nu_{min})$ and $z^+(95\% Nu_{ss})$ for the case of Ra = 6450 and 3780. It is found that θ_m when plotted against z^+ is independent of both Ra and Re over the range of our investigation with the greatest difference between θ_m for forced convection and θ_m for mixed convection being less than 1.5%. The minimum

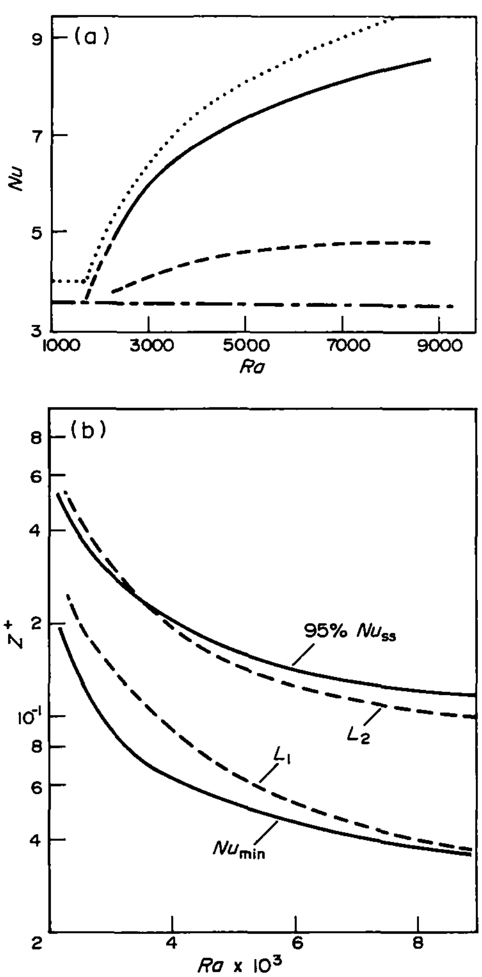

FIG. 7. (a) Nu_{ss} (solid line) and Nu_{min} (broken line) vs Ra. The dotted line corresponds to Nu_{ss} of mixed convection between two flat plates [19], (b) Variations of $z^+(95\% Nu_{ss})$, $z^+(Nu_{min})$, $z^+_{L_1}$ and $z^+_{L_2}$ with Ra.

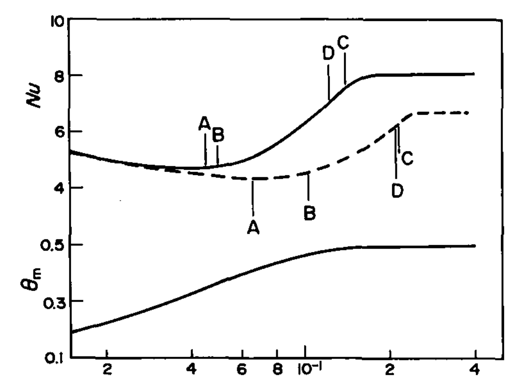

FIG. 8. Developments of Nu (solid line for Ra = 6446; broken line for Ra = 3789) and non-dimensional mixed mean fluid temperature, θ_m, with z^+. $A = z^+(Nu_{min})$, $B = z^+_{L_1}$, $C = z^+(95\% Nu_{ss})$, $D = z^+_{L_2}$.

Nusselt number occurs in the region where T_m is developing. When Ra is low, the entrance length L_1 is in the region in which θ_m is close to its final value of 0.5 (i.e. the average temperature of the top and the bottom plates). As the Rayleigh number is increased, L_1 shifts upstream to the region in which T_m is rising sharply. On the other hand, L_2 is always located in the region where θ_m is very close to its final value of 0.5.

SUMMARY AND CONCLUSIONS

A thermally-developing nitrogen gas flow in a rectangular duct with $AR = 10$ is studied numerically for the case in which the top and the bottom boundaries are respectively cooled and heated isothermally with adiabatic (or cooled) sidewalls. The present analysis, which shows good agreement with the experimental results of Chiu and Rosenburger, and Chiu *et al.*, focuses on the following two objectives; (1) examination of flow structure, such as the onset and the full development of mixed convection, in relation to thermal transport, and (2) investigation of the effects of various parameters, such as the Rayleigh number, and the relative magnitudes of boundary- as well as inlet-gas temperatures on flow and heat transfer at the entrance region of a rectangular duct. Specific conclusions are:

(1) Over the range of $\sim 2500 < Ra < \sim 8500$, in which steady mixed convection prevails, the inverse Graetz number, $z^+_{L_1}$ (for the onset of mixed convection) as well as $z^+_{L_2}$ (for the full development of mixed convection) may be used to present the entrance lengths as functions of Ra only, indicating that the physical dimensions and the flow velocity merely stretch or contract the flow and thermal variations in the streamwise direction. Equations for L_1 and L_2, developed from the present analyses, are given as equations (13) and (14) respectively.

(2) $z^+(Nu_{min})$ (=the location where Nu takes a minimum) and $z^+(95\% Nu_{ss})$ (=the location where Nu reaches 95% of its fully-developed value) are also functions of Ra alone; while, the non-dimensional mixed mean fluid temperature, $\theta_m = \theta_m(z^+)$, is found to be independent of Ra for a duct with $AR = 10$. In terms of thermal transport, $z^+_{L_1}$ and $z^+_{L_2}$ are located near $z^+(Nu_{min})$ and $z^+(95\% Nu_{ss})$, respectively. Since Nu_{min} occurs far downstream from the location where the Nusselt number starts to deviate from the corresponding Nusselt number for forced convection, this provides an explanation for the discrepancy between the experimental results and the theoretical prediction on the onset of mixed convection.

(3) Nu_{ss} for our case of $AR = 10$ is lower than the corresponding value for mixed convection between two horizontal plates by 8–10%, indicating that the sidewall effects are still important in examining thermofluid structure of high aspect ratio ducts.

(4) When the inlet gas temperature is lower or higher than the temperature of the top boundary, both L_1 and L_2 change accordingly. Examination of the development of velocity profiles reveals that the location of $z^+_{L_1}$ is affected by the magnitude of the inlet gas temperature relative to the top wall, whereas, the development of mixed convection from $z^+_{L_1}$ to $z^+_{L_2}$ is not affected to a significant degree, indicating that the changes in L_1 and L_2 are mostly due to initial enhancement or suppression of the buoyancy-induced flow.

(5) When the sidewall is kept at a specified temperature ($T_s = T_{top}$), fully-developed mixed convection consists of six roll cells over the half-width, instead of five for the case of the adiabatic sidewalls although the entrance lengths, L_1 and L_2, are only slightly shorter than the corresponding values for the case of the adiabatic sidwalls.

Acknowledgement—The author wishes to express his gratitude for the Research Division, KOMATSU Ltd., Hiratsuka, Japan, where the major portion of this study was performed during his sabbatical leave. Gratitude is also extended to the A. & J. Whiting Foundation for defraying the cost of travel.

REFERENCES

1. G. S. Beavers, E. M. Sparrow and R. A. Magnusson, Experiments on hydrodynamically developing flow in rectangular ducts of arbitrary aspect ratio, *Int. J. Heat Mass Transfer* **13**, 689–702 (1970).
2. R. K. Shah and A. L. London, Laminar flow forced convection in ducts. *Advances in Heat Transfer*, Suppl. 1. Academic Press, London (1978).
3. M. Akiyama, G. J. Hwang and K. C. Cheng, Experiments on the onset of longitudinal vortices in laminar forced convection between horizontal plates, *J. Heat Transfer* **93**, 335–341 (1971).
4. G. J. Hwang and K. C. Cheng, Convective instability in the thermal entrance region of a horizontal parallel-plate channel heated from below, *J. Heat Transfer* **95**, 72–77 (1973).
5. Y. Kamotani and S. Ostrach, Effect of thermal instability on thermally developing laminar channel flow, *J. Heat Transfer* **98**, 62–66 (1976).
6. Y. Kamotani, S. Ostrach and H. Miao, Convective heat transfer augmentation in thermal entrance regions by means of thermal instability, *J. Heat Transfer* **101**, 222–226 (1979).
7. F. P. Incropera and J. A. Schutt, Numerical simulation of laminar mixed convection in the entrance region of horizontal rectangular ducts, *Numerical Heat Transfer* **8**, 707–729 (1985).
8. K. Chiu and F. Rosenberger, Mixed convection between horizontal plates—I. Entrance effects, *Int. J. Heat Mass Transfer* **30**, 1645–1654 (1987).
9. J. Ou, K. C. Cheng and R. Lin, Natural convection effects on Graetz problem in horizontal rectangular channels with uniform wall temperature for large *Pr*, *Int. Heat Mass Transfer* **17**, 835–843 (1974).
10. M. M. M. Abou-Ellail and S. M. Morcos, Buoyancy effects in the entrance region of horizontal rectangular channels, *J. Heat Transfer* **105**, 924–928 (1983).
11. K. Chiu, J. Ouazzani and F. Rosenberger, Mixed convection between horizontal plates—II. Fully developed flow, *Int. J. Heat Mass Transfer* **30**, 1655–1662 (1987).
12. H. K. Moffat and K. F. Jensen, Complex flow phenomena in MOCVD reactors. I. Horizontal reactors, *J. Crystal Growth* **77**, 108–119 (1986).

13. H. K. Moffat and K. F. Jensen, Three-dimensional flow effects in silicon CVD in horizontal reactors, *J. electrochem. Soc.*, **135**, 459–471 (1988).
14. K. F. Jensen, D. I. Fotiadis, H. K. Moffat, E. O. Einset, A. M. Kremer and D. R. McKenna, Fluid mechanics of chemical vapor deposition. In *Interdisciplinary Issues in Materials Processing and Manufacturing* (Edited by S. K. Samanta *et al.*), Vol. 2, pp. 565–586. ASME Winter Annual Meeting, Boston (1987).
15. K. F. Jensen, E. O. Einset and D. I. Fotiadis, Flow phenomena in chemical vapor deposition of thin films. In *Annual Review of Fluid Mech.* **23**, 197–232. Annual Reviews Inc. (1991).
16. R. Chilukuri and R. H. Pletcher, Numerical solutions to the partially parabolized Navier–Stokes equations for developing flow in a channel, *Numerical Heat Transfer* **3**, 169–188 (1980).
17. S. V. Patankar, *Numerical Heat Transfer and Fluid Flow*. Hemisphere, New York (1980).
18. G. E. Willis and J. W. Deardorff, The oscillatory motion of Rayleigh convection, *J. Fluid Mech.* **44**, 617–672 (1970).
19. K. Fukui, M. Nakajima and H. Ueda, The longitudinal vortex and its effects on the transport processes in combined free and forced laminar convection between horizontal and inclined parallel plates, *Int. J. Heat Mass Transfer* **26**, 109–120 (1983).